Nano Energy 97 (2022) 107193

Contents lists available at ScienceDirect

Nano Energy

journal homepage: www.elsevier.com/locate/nanoen

Multi-site passivation-based antisolvent additive engineering with gradient distribution for superior triple cation P-I-N perovskite solar cells

Yu-Jin Kang, Seok-In Na *

Department of Flexible and Printable Electronics and LANL-JBNU Engineering Institute-Korea, Jeonbuk National University, 567, Baekje-daero, Deokjin-gu, Jeonju-si, Jeollabuk-do 54896, Republic of Korea

ARTICLE INFO

Keywords:
Perovskite solar cells
Additive engineering
Anti-solvent additive engineering
Multi-functional additives
Defect passivation

ABSTRACT

The large number of diverse types of trap sites on the surface and inside perovskite substantially restrict the production of highly efficient and stable perovskite solar cells (PSCs). Therefore, it is essential to fabricate high-quality perovskite films via the passivation of multi-site defects at the surface and grain boundaries through modulating perovskite crystallization and passivating as many defects of perovskite films as possible. Although many passivation molecules have been reported, it is still necessary to develop a deeper understanding of the various functional group effects as well as the different passivation strategies that can be used to introduce additives. Here, to confirm the effects of functional groups, the four acrylate-based molecules that contain carbonyl (C═O), hydroxyl (–OH), alkoxy (–O–CH_2), or aromatic functional group are used as additives for antisolvent additive engineering (AAE). We then systematically investigate the effects of the passivation molecules on perovskite films and devices. The use of the optimum multi-functional additive, 3-Phenoxy-2-hydroxypropyl acrylate (PHA), enables a champion power conversion efficiency (PCE) of 20.72% as well as higher ambient air stability, as it retains over 51% of its initial PCE after 129 days. We also find that, compared to other representative passivation techniques, AAE containing passivation molecules leads to better perovskite films with a lower defect density and better photovoltaic performance. Consequently, the multi-type defects caused by the ionic properties of perovskite are substantially reduced due to the synergetic effects of the functional groups; further, the AAE approach has also proven to be a more promising way to obtain high-quality perovskite films corresponding to high-efficiency PSCs.

1. Introduction

In recent years, organic-inorganic hybrid PSCs that have a unique structure of ABX_3 (where the A site is monovalent organic/inorganic cations (Methylammonium ($CH_3NH_3^+$, MA^+), Formamidinium ($NH_2CHNH_2^+$, FA^+), Cs^+, and Rb^+), the B site is smaller divalent metal ions (Pb^{2+} and Sn^{2+}), and the X site is generally a halide ion (Cl^-, Br^-, and I^-)) have shown tremendously improved efficiency from 3.9% to 25.7% [1–4]. As the perovskite's remarkable optoelectronic properties—such as high efficiency, good charge carrier mobility, long intrinsic carrier recombination lifetime, long electron and hole diffusion length, simply tunable band gap, and high absorption coefficient in visible light range—have become increasingly well known, PSCs have come to be considered one of the most promising next-generation alternatives to Si-based solar cells, and they have been examined by many researchers [5–8]. However, due to the solution-processing and the nature of polycrystalline, PSCs can contain various types of defects (undercoordinated Pb^{2+}, undercoordinated halide ions (X^-), ion vacancies (I^-, MA^+), etc.) that induce charge recombination and ion migration at the surface and inside the perovskite absorber, thus limiting the implementation of highly efficient and stable PSCs [9–11].

Therefore, removing the defects that detrimentally affect perovskite is a key aspect of improving the photovoltaic performance and the device stability. As a result, there have been numerous attempts to produce high-performance PSCs through defect passivation and the control of grain growth. Among them, additive engineering—which involves adding an effective agent into perovskite—is known to be a simple and effective method [12–14]. Additives with various functional groups (C═O, –OH, Cl^-, NH_3^+, aromatic ring, etc.) can effectively eliminate defects and prevent ion migration through electrostatic interactions with perovskite via coordination bonds or ionic bonds. Specifically, to passivate the dense and diverse types of defects, the passivation

* Corresponding author.
E-mail address: nsi@jbnu.ac.kr (S.-I. Na).

https://doi.org/10.1016/j.nanoen.2022.107193
Received 27 January 2022; Received in revised form 16 March 2022; Accepted 24 March 2022
Available online 27 March 2022

molecule structure with multi-functional groups has been studied and developed beyond one functional group. Defect passivation and crystal growth control through the integrated effects of various functional groups have been shown to be effective in improving the photovoltaic performances and long-term stability of devices [15–17]. For example, Huang et al. newly introduced D-4-tert-butylphenylalanine (D4TBP) having carboxyl (–COOH), amine (–NH_2), and aromatic groups, and they showed that this structure could reduce the multiple kind of defects via ionic and coordination interaction and considerably improve the photovoltaic performance with a small V_{OC} deficit [15]. In another study, Xu et al. introduced multi-functional molecules by tailoring an amine group (–NH_2), a carbonyl group (C═O), and a benzene ring with a halogen functional group (F, Cl), and this method was shown to be effective in passivating negatively and positively charged defects [16].

Even though research into multi-functional additives has shown them to be extremely effective and necessary for defect passivation and grain growth, there have been few in-depth studies investigating the functional groups and their effects on perovskite films and their photovoltaic performances. To date, most functional additives have been shown to only passivate one or two types of defects in perovskite, and to only control either the defects or the perovskite crystallization. It also remains unclear which and how many functional groups lead to the best outcomes in multi-function additives with complex structures. Therefore, there are still unsettled research considerations regarding molecular configurations with better functional groups. In addition, although there has been some research showing that the antisolvent additive engineering (AAE) process could be a better approach for the production of PSCs devices [18–21], there have been almost no in-depth studies examining multi-functional additives, unlike the trials in conventional passivation methods. Moreover, although the passivation effects of the additives in and/or on perovskite films could be differ substantially with the passivation processes used and the substantial additive's distribution, there have yet to be any studies aiming for a deeper understanding of AAE itself or conducting practical comparisons of AAE with other representative passivation processes (additive engineering and surface post-treatment).

In this study, as promising and novel multi-functional additives for AAE, we introduced 2-hydroxyethyl acrylate (HA), Benzyl acrylate (BA), 2-Phenoxyethyl acrylate (PA), and 3-Phenoxy-2-hydroxypropyl acrylate (PHA) having carbonyl (C═O), hydroxyl (–OH), alkoxy (–O–CH_2), or/and aromatic functional groups, because each of these well-known groups can be compared and combined with the effects: the C═O functional group can passivate under-coordinated Pb^{2+} defects while filling the halide vacancy, and it can also modulate perovskite crystallization; the –OH functional group can interact with positively and negatively charged defects via hydrogen bonding and coordination bonding, which can promote the quality of the perovskite film through the center of nucleation; the –O–CH_2 group can form a hydrogen bond with organic species (MA^+, FA^+) with enhanced device stability, and the oxygen atom containing an unshared electron pair can also act as a Lewis base passivator; and the higher electron cloud density on the aromatic functional group can reduce the accepter type trap state, thus leading to a better passivation effect [15,22–26]. In this study, we systematically investigated the effects of multi-functional additives on photovoltaic performances, charge transport dynamics, and changes in perovskite surface and film. A comprehensive investigation revealed which functional groups work and how they combine with the abundant defects in the perovskite. The results indicated that the synergistic effects of each functional group can produce high quality perovskite films with a larger grain size and higher crystallinity along with substantially reduced defect density. Among the investigated multi-functional molecules, we find that a new type of passivation molecule—PHA, which has all four effective passivation groups (C═O, –OH, –O–CH_2, and aromatic)—leads to the greatest increase in charge carrier behavior, reduction in defect density, and improvement in crystallinity and grain growth. Further, PHA was confirmed to be applicable to various passivation processes; among them, the best performance improvement was seen when PHA was adopted in the antisolvent additive process (AAE). As a result, PSCs applied with PHA showed a significant increase in average PCE from 17.50% to 19.61%, and they achieved the highest PCE of 20.72% with low open-circuit voltage (V_{OC}) loss. Further, the PHA-adopted PSCs also exhibited long-term stability, as they maintained over 38% of their initial PCE after exposure to ambient air conditions for 189 days.

2. Results and discussion

To assess the differential effects of passivation molecules with various functional groups on the device performance, inverted planar-structured PSCs were adopted (Fig. 1a). In the fabrication process we used, additives were injected into the toluene-based anti-solvent at the optimal concentration and deposited onto the pristine perovskite films during the spin-coating, as shown in Fig. 1b. To systematically investigate the passivation effects of functional groups, four acrylate-based molecules were selected: 2-hydroxyethyl acrylate (HA), Benzyl acrylate (BA), 2-Phenoxyethyl acrylate (PA), and 3-Phenoxy-2-hydroxypropyl acrylate (PHA) (Fig. 1c).

The photovoltaic characteristics of the different passivation molecules were measured at the optimal concentrations of the passivation molecules to confirm the effects of different passivation molecules with functional groups and to determine the optimum passivation agent for AAE. The PCE distributions with and without passivation molecules are shown in Fig. 2a, and the other PSCs parameters are summarized in Fig. S1 and Table S1. Comparing the normal antisolvent strategy, the devices adopting AAE-based-passivation molecules showed improved results in all parameters: the PSCs with HA, BA, PA, and PHA showed significant improvements in average PCE from 17.50% to 18.72%, 18.88%, 19.11%, and 19.61%, respectively, and their V_{OC}, J_{SC}, and FF all increased as well. Fig. 2b and Table 1 present the representative device parameters with and without passivation molecules. In contrast to the pristine PSCs, the representative device parameters with HA, BA, PA, and PHA showed increased PCE values from 18.40% to 19.50%, 19.77%, 20.00%, and 20.72%, respectively; respective increases in V_{OC} from 1.069 V to 1.126 V, 1.122 V, 1.132 V, and 1.153 V; respective increases in J_{SC} from 22.38 mA cm^{-2} to 22.44 mA cm^{-2}, 22.68 mA cm^{-2}, 22.66 mA cm^{-2}, and 23.06 mA cm^{-2}; and respective increases in FF from 76.90% to 77.21%, 77.73%, 77.97%, and 77.93%. It is particularly noteworthy that the devices manufactured by PHA achieved the highest efficiency, which is mainly attributed to the noticeable increase in V_{OC}. As shown in Fig. 2c, the external quantum efficiency (EQE) measurements also confirm these improvements in the photovoltaic characteristics. These EQE spectrums of the PSCs with passivation molecules denote higher photon-to-current conversion efficiencies than the pristine PSC over the overall spectral ranges. In addition, to further investigate the internal quantum efficiency (IQE) of the devices, the IQE spectra of the PSCs with and without passivation molecules were obtained using the following formula (1) [27]:

$$\mathrm{EQE} = \text{absorption efficiency}(n_A) \times \mathrm{IQE} \quad (1)$$

When compared to pristine PSCs, PSCs with passivation molecules also showed higher measured IQE under the overall spectra. In particular, the EQE and IQE improvement ratios of HA-, BA-, PA-, and PHA-adopted PSCs showed similar values, thus indicating that the PCE enhancements obtained by the multifunctional additives were principally due to the improvements in charge extraction and transport capabilities [28].

To further investigate the charge carrier behavior of the PSCs with passivation molecules, the following relationships were examined: the dependence of V_{OC} on the light intensities, and photo-generated charge carrier extraction by linearly increasing voltage (photo-CELIV), transient photovoltage (TPV), and transient photocurrent (TPC). Fig. 3a illustrates the dependence of V_{OC} on the light intensities of the PSCs with

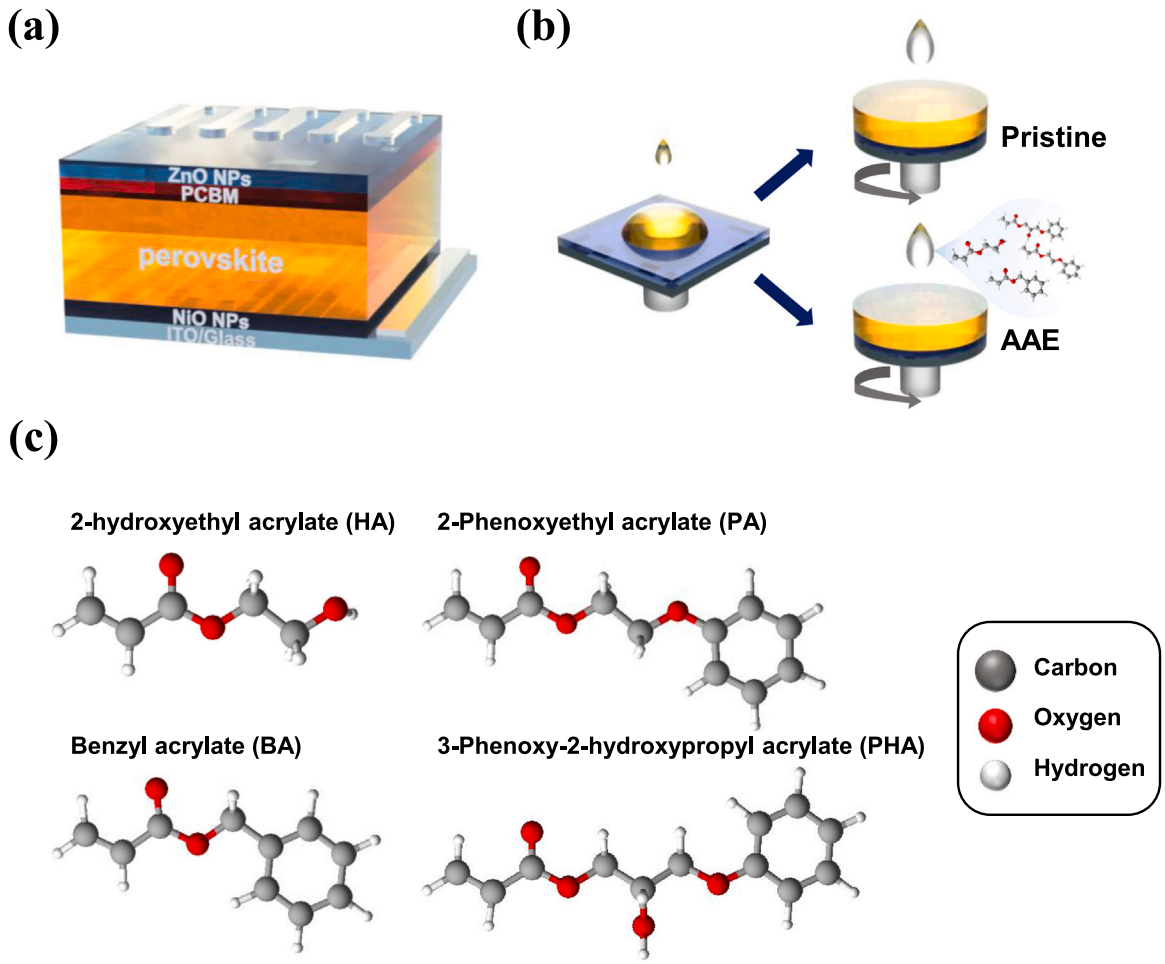

Fig. 1. (a) Schematic structure of inverted planar perovskite solar cell (ITO/NiO NPs/perovskite/PCBM/ZnO NPs/Ag). (b) Pristine anti-solvent process and AAE with different passivation agents. (c) Chemical structures of passivation molecules with different functional groups.

and without passivation molecules. The recombination strength occurring inside PSCs is represented by the liner relationship between V_{OC} and light intensities, which can be calculated using Eq. (2)[29,30]:

$$V_{OC} = n\frac{kT}{e}\ln(I) + \text{constant} \quad (2)$$

Where *n, e, k,* and *T* are the ideal factor, elementary charge, Boltzmann constant, and absolute temperature, respectively. When the *n* value is 1, it indicates linear dependence and reduced charge carrier recombination. We can therefore elucidate the interior recombination mechanism of PSCs by linearly plotting V_{OC} as a function of log-scaled light intensities [29–31]. The pristine PSC has a slope of 1.514 kT/q, while the devices with HA, BA, PA, and PHA have smaller slopes of 1.448 kT/q, 1.425 kT/q, 1.406 kT/q, and 1.365 kT/q, respectively, suggesting that the passivation molecules can reduce the trap-assisted recombination and the recombination strength. The reduced recombination is also consistent with the noticeable increase in the V_{OC}.

To verify the charge carrier transport in PSCs under the operating conditions, photo-CELIV data was collected, and it is shown in Fig. 3b. The charge carrier mobility of PSCs with and without passivation molecules can be obtained as follows using Eq. (3) [32,33]:

$$\mu = \frac{2d^2}{3\frac{\Delta U}{\Delta t}t_{max}^2} \quad (3)$$

where μ is the charge mobility, $\Delta U/\Delta t$ is the voltage ramp of the applied triangle voltage pulse, t_{max} is the time when the value of the current density is at its maximum, and d is the thickness of the perovskite film.

The charge carrier mobilities with HA, BA, PA, and PHA were 9.565×10^{-3} cm^2 V^{-1} s^{-1}, 9.565×10^{-3} cm^2 V^{-1} s^{-1}, 1.084×10^{-2} cm^2 V^{-1} s^{-1}, and 1.157×10^{-2} cm^2 V^{-1} s^{-1}, respectively, all of which are higher than that of the PSCs without passivation molecules (8.503×10^{-3} cm^2 V^{-1} s^{-1}). This suggests that the AAE-adopted passivation molecules promote quicker charge carrier mobility in perovskite films [28]. In addition, to further elucidate the charge carrier dynamics in PSCs with passivation molecules, TPV and TPC measurements were taken under operation conditions and calculated using a bi-exponential decay function, as shown in Fig. 3c–d. The TPV decay times of PSCs with HA, BA, PA, and PHA increased from 110 μs (pristine) to 287 μs, 329 μs, 729 μs, and 1549 μs, respectively, thus indicating increased charge carrier recombination lifetime and reduced charge carrier recombination. In addition, the TPC decay times of PSCs with HA, BA, PA, and PHA were 0.453 μs, 0.407 μs, 0.398 μs, and 0.359 μs, respectively, all of which are faster than that of the PSCs without passivation molecules (0.471 μs). These results confirm that the passivation molecules lead to much more efficient charge transport and extraction [34]. Therefore, the overall improved PSC performances can be attributed to the better charge transport capacities with effectively reduced charge carrier recombination caused by defects.

Scanning electron microscopy (SEM) and X-ray diffraction (XRD) analyses were conducted to further investigate the effects that the adoption of the different passivation molecules via AAE had on the morphology and crystal growth in the perovskite films. Fig. 4a shows the surface and cross-sectional SEM images of perovskite films according to the different passivation molecules. When passivation molecules were

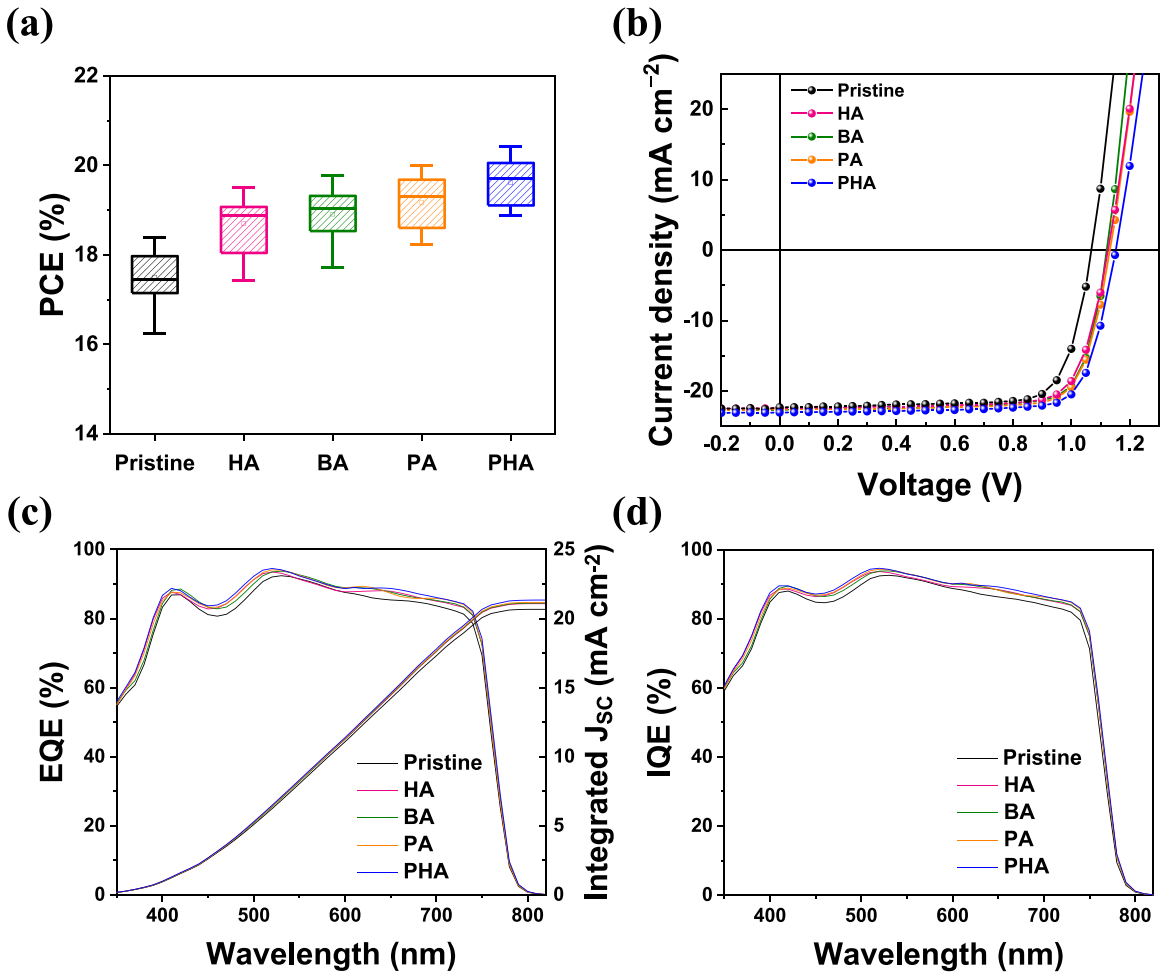

Fig. 2. (a) Statistical distribution of PCE according to different passivation molecules. (b) Representative J-V curves, (c) EQE curves and integrated J_{SC}, and (d) IQE curves of PSCs with and without different passivation molecules.

Table 1
Representative photovoltaic parameters of PSCs with and without different passivation molecules under standard AM 1.5 G illumination (100 mW cm^{-2}).

Best	V_{OC} (V)	J_{SC} (mA cm^{-2})	FF (%)	PCE (%)
Pristine	1.069	22.38	76.90	18.40
HA	1.126	22.44	77.21	19.50
BA	1.122	22.68	77.73	19.77
PA	1.132	22.66	77.97	20.00
PHA	1.153	23.06	77.93	20.72

introduced into the perovskite films, the grain size of perovskite was clearly changed in the SEM images, whereas the thicknesses of the perovskite layer with and without passivation molecules are similar at about 450 nm. Compared to the pristine perovskite film, the average surface SEM grain sizes of HA, BA, PA, and PHA increased from 139.36 nm (pristine) to 179.41 nm, 204.88 nm, 217.49 nm, and 250.84 nm, respectively, and the cross-sectional grain boundaries were reduced substantially with the passivation molecules. Fig. 4b clarifies the effect of passivation molecules in perovskite film crystallization. The intensities of the main perovskite diffraction peaks (110) and (220), which are respectively located at 14.1° and 28.4°, are stronger than those of the pristine films with no new peaks and no peak shifts, indicating that the highly crystallized perovskite's phase did not have a lattice change of perovskite [35–37]. This is also supported by the sharp and narrow full width at half maximum (FWHM) of the (110) diffraction peak; the FWHM values with HA, BA, PA, and PHA were decreased to 0.22, 0.22, 0.21, and 0.19, respectively (compared to the pristine value of 0.25), suggesting that the introduction of passivation molecules can have positive effects on the crystallization of the perovskite films [38]. Further, as shown in Fig. S2, the atomic force microscope (AFM) analysis denoted that the surface roughness (RMS) also decreased with the addition of the passivation molecules. These results show that the passivation molecules can play a significant role in grain growth with smaller grain boundaries, enhancing the crystallinity of perovskite, and enabling smooth and dense perovskite films, all of which facilitate charge carrier transportation and enhance overall photovoltaic performance [39]. To further examine the light absorption and charge carrier behaviors in the perovskite films, ultraviolet-visible spectroscopy (UV–vis), steady-state photoluminescence (PL), and space-charge-limited current (SCLC) measurements were conducted. As shown in Fig. S3, the UV–vis absorption spectra display no apparent differences between pristine perovskite film and perovskite films with passivation molecules over the entire visible spectral range, thus indicating that the films have similar light absorption abilities. This finding is consistent with the finding showing that the increased EQE and IQE were mainly obtained as a result of the improved charged carrier extraction and transport, rather than an increase in the light absorption [27]. More significantly, as demonstrated in the PL data of Fig. 4c, the perovskite films with passivation molecules exhibited a considerably stronger peak intensity than the pristine films, suggesting that non-radiative recombination was substantially reduced in the perovskite films with AAE-based passivation molecules [37]. Moreover, the PL peaks of the passivation molecules-adopted perovskite films have a

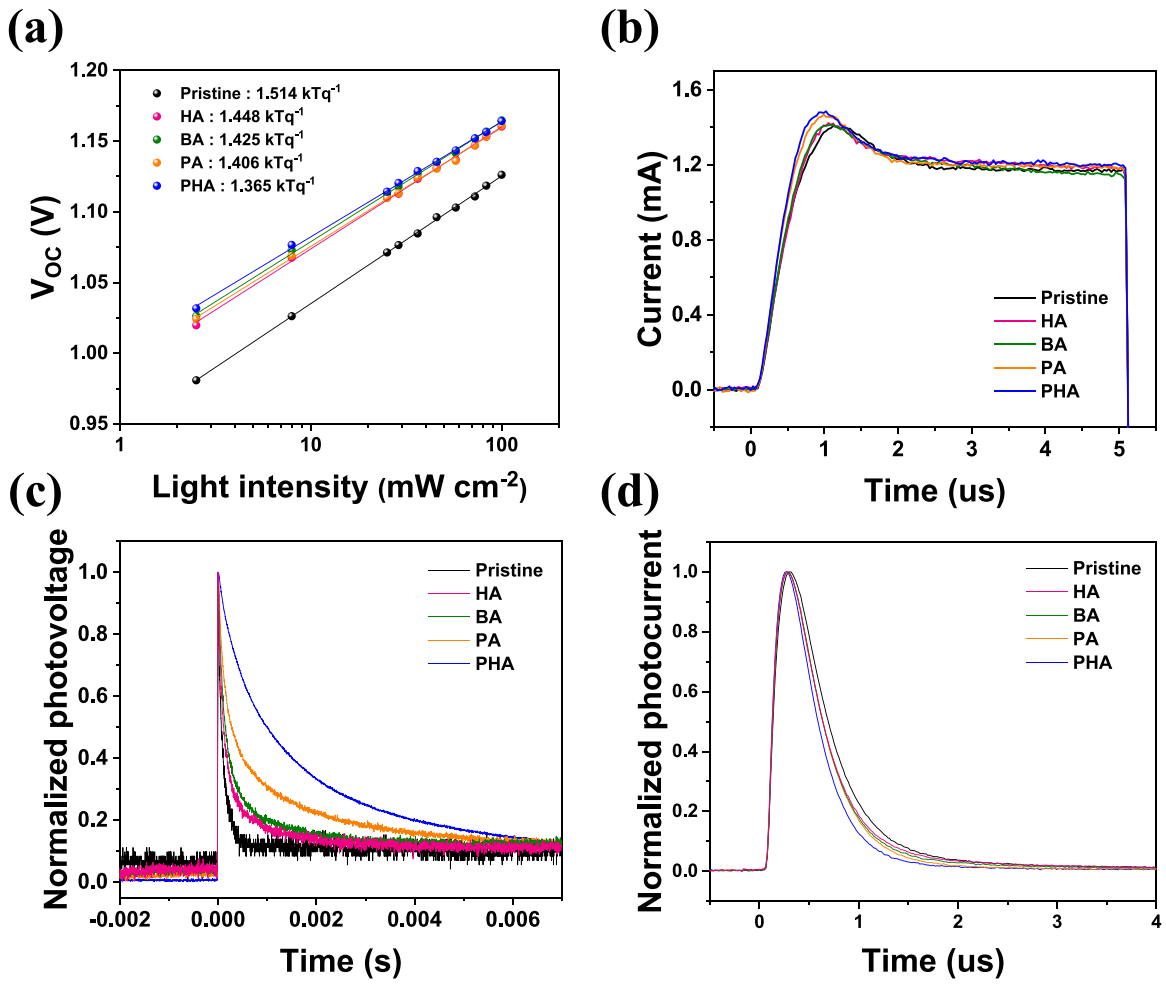

Fig. 3. (a) Dependence of V_{OC} on the light intensities, (b) Photo-CELIV measurement, (c) TPV, and (c) TPC of PSCs with and without different passivation molecules.

slight blue-shift, implying a decrease in the trap density through the successful passivation and/or inhibition of the defects in the perovskite films [37,40,41]. We also conducted SCLC measurements to validate the defect density in perovskite films with and without passivation molecules, and the results are shown in Fig. 4d–h. The defect density was calculated according to the following Eq. (4) [41]:

$$N_{defects} = \frac{2\varepsilon\varepsilon_0 V_{TFL}}{eL^2} \quad (4)$$

where N_{defecs} is the trap density; ε is a relative dielectric constant (28.8 for perovskite); ε_0 is the vacuum permittivity; V_{TFL} is the trap-filled limited voltage, which is an intersection between ohmic and TFL fitting curves; e is the elementary charge; and L is the thickness of the perovskite film [41,42]. The obtained V_{TFL} values of perovskite with HA, BA, PA, and PHA were decreased from 0.80 V (pristine) to 0.50 V, 0.40 V, 0.31 V, and 0.26 V, respectively, and we can thus find that the defect densities with passivation molecules were decreased as well. These findings suggest that the passivation molecules can ameliorate the perovskite film quality through higher crystallinity, larger grain size, and remarkably reduced defect densities, ultimately leading to an improvement in the overall performance of the PSCs.

To understand how passivation molecules lead to beneficial changes in PSCs and which functional group is the one primarily working, we measured the Fourier transform infrared (FT-IR) spectra of HA, BA, PA, PHA, and perovskite precursor solution with passivation molecules. As shown in Fig. 5a, pure HA, BA, PA, and PHA all exhibit the same characteristic peaks of C═O at around 1720 cm^{-1}. When the passivation molecules (HA, BA, PA, and PHA) were added to the perovskite precursor, the vibration peaks of C═O bond were respectively slightly shifted from 1721, 1721, 1722, and 1722 cm^{-1} to 1720, 1719, 1721, and 1720 cm^{-1}. Further, Figs. 5b and S4a show that the C═C vibrations (aromatic ring) of BA, PA, and PHA in perovskite precursor solution were respectively slightly moved from 1498, 1496, and 1495 cm^{-1} to 1497, 1492, and 1492 cm^{-1}. The –OH vibrations of HA and PHA in perovskite precursor solution were also respectively noticeably moved from 3420 and 3445 cm^{-1} to 3325 and 3318 cm^{-1} (Figs. 5c and S4b). Further, when HA, BA, PA, and PHA were added into the perovskite solution, as shown in Fig. S4c, the C–O vibrations (ester) of HA, BA, PA, and PHA showed a slight shift to the lower side. By contrast, Figs. 5d and S4d show that the C–O vibrations (aromatic ether) of PA and PHA were shifted toward higher frequencies (from 1243 and 1241 cm^{-1} to 1252 and 1249 cm^{-1}), which could be caused by the reinforcement of the C–O bond and/or another underlying interaction between perovskite and other functional groups located nearby, rather than the interaction of the O atom next to the benzene ring with the perovskite [43,44]. More importantly, synthetically, these low shifts of stretching vibrations represent the interaction between perovskite and functional groups, particularly the proactive and practical functional groups acting as Lewis bases that can interact with Lewis acids such as PbI_2 and consequently form adducts [20,45–47]. From this perspective, it can be deduced that the addition of the functional molecules via AAE into the perovskite could selectively form an intermediate phase by providing an electron pair from the functional groups (C═O, aromatic ring, –OH, and C–O (ester)) to the under-coordinated Pb^{2+} or organic cations. This can promote crystal growth and the nucleation center, which is assisted by

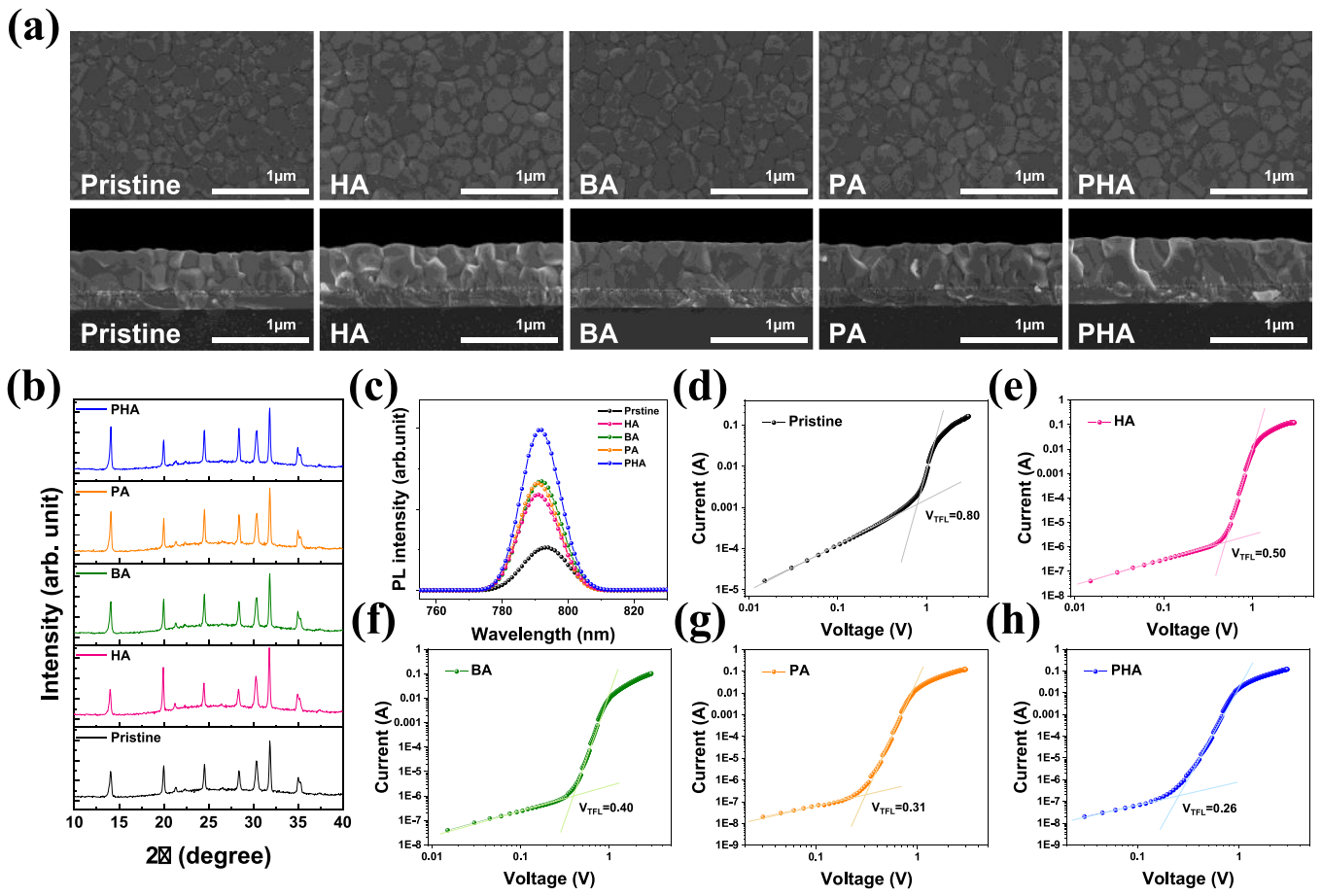

Fig. 4. (a) Surface and cross-sectional SEM images, (b) XRD patterns, and (c) PL spectra of perovskite films for Pristine, HA, BA, PA, and PHA. Current density-voltage curves of devices (ITO/Perovskite/Au): (d) Pristine perovskite and perovskite with (e) HA, (f) BA, (g) PA, and (h) PHA.

the enlarged perovskite grains, as verified by the SEM results above. Further, larger perovskite grains indicate that more functional groups work more effectively to improve nuclear growth, which can concurrently diminish the grain boundaries of perovskite and the defects generated by these boundaries, thereby moderating the charge recombination and enhancing the charge transfer characteristics. X-ray photoelectron spectroscopy (XPS) measurements were further conducted to verify the chemical interactions between the perovskite and the organic passivation molecules (Fig. S5a). As shown in Fig. 5e, when adding the passivation molecules to the pristine perovskite films, the characteristic peaks of Pb 4 $f_{7/2}$ and 4 $f_{5/2}$ are shifted toward lower binding energies than those of the pristine perovskite film (with respective values of 138.35 eV and 143.19 eV, 138.23 eV and 143.10 eV, 138.31 eV and 143.20 eV, 138.45 eV and 143.30 eV, and 138.53 eV and 143.39 eV; (Pb 4 $f_{7/2}$) and (Pb 4 $f_{5/2}$) for PHA, PA, BA, HA, and Pristine, respectively), and the characteristic peaks of I $3d_{5/2}$ and $3d_{3/2}$ also showed a similar tendency (Fig. S5b). These shifts indicate that there were interactions between passivation molecules and perovskite through the coordination and hydrogen bonds, thus implying that the charged defects could be electrostatically passivated after adding the passivation molecules. More specifically, the decrease in the binding energies of the core-level electrons was attributed to the increased electron cloud density of Pb due to the donation of the lone electron pair from the passivation molecules [48]. As a result, the decrease in the binding energy of the core-level electrons indicates that the valence electrons of Pb were less involved in the Pb-I bond and that the oxidation state of Pb can be reduced, which also lower the oxidation state of I [49,50]. Further, the relative increase in binding energy could be due to a decrease in the electron cloud density of I through the hydrogen bonding of the hydroxyl group passivating the halogen anion (I, Br) [51,52]. Synthetically, these shifts can be induced by the chemical interaction of C═O→Pb^{2+}, C–O (ester)→Pb^{2+}, aromatics→FA^{+} and/or MA^{+}, –OH→Pb^{2+}, and –OH→I^{-} [53]. Further, as shown in Fig. S5c, the characteristic peaks of N 1 s showed lower shifts except for HA, which originates from the interaction between the electron-rich benzene rings of BA, PA, and PHA, and organic cations [26,54]. These results are also consistent with the IR results described earlier. Thus, when combining the above FT-IR and XPS data, it can be determined that the functional groups of passivation molecules can minimize defect density by selectively interacting with the positively or negatively charged defects in perovskite, which allow perovskite grains to grow bigger while passivating the grain boundaries and surface of the perovskite. Accordingly, it was possible to infer whether or not each functional group worked, as well as the strength of defect passivation. Among the passivation molecules, PHA with various functional groups had the most interaction with perovskite, which ultimately leads to improved overall photovoltaic performance. It can also be deduced that the increased efficiency is related not only to the passivation of the perovskite surface, but also to the suppression of charge recombination caused by the lower defect density that stems from the growth of better perovskite crystals when passivation molecules are used. The environmental stability of PSCs is a critical issue for their further practical implementation. PSCs are easily decomposed by moisture, oxygen, and heat under ambient conditions, and various defects present in the perovskite films and grain boundaries make them susceptible to oxygen and moisture in the air. First, we took XRD measurements of perovskite films with and without different passivation molecules under air atmosphere conditions (30 ± 5 ℃, 45 ± 5% relative humidity (RH)), as shown in Figs. 5f and S6. After 70 days

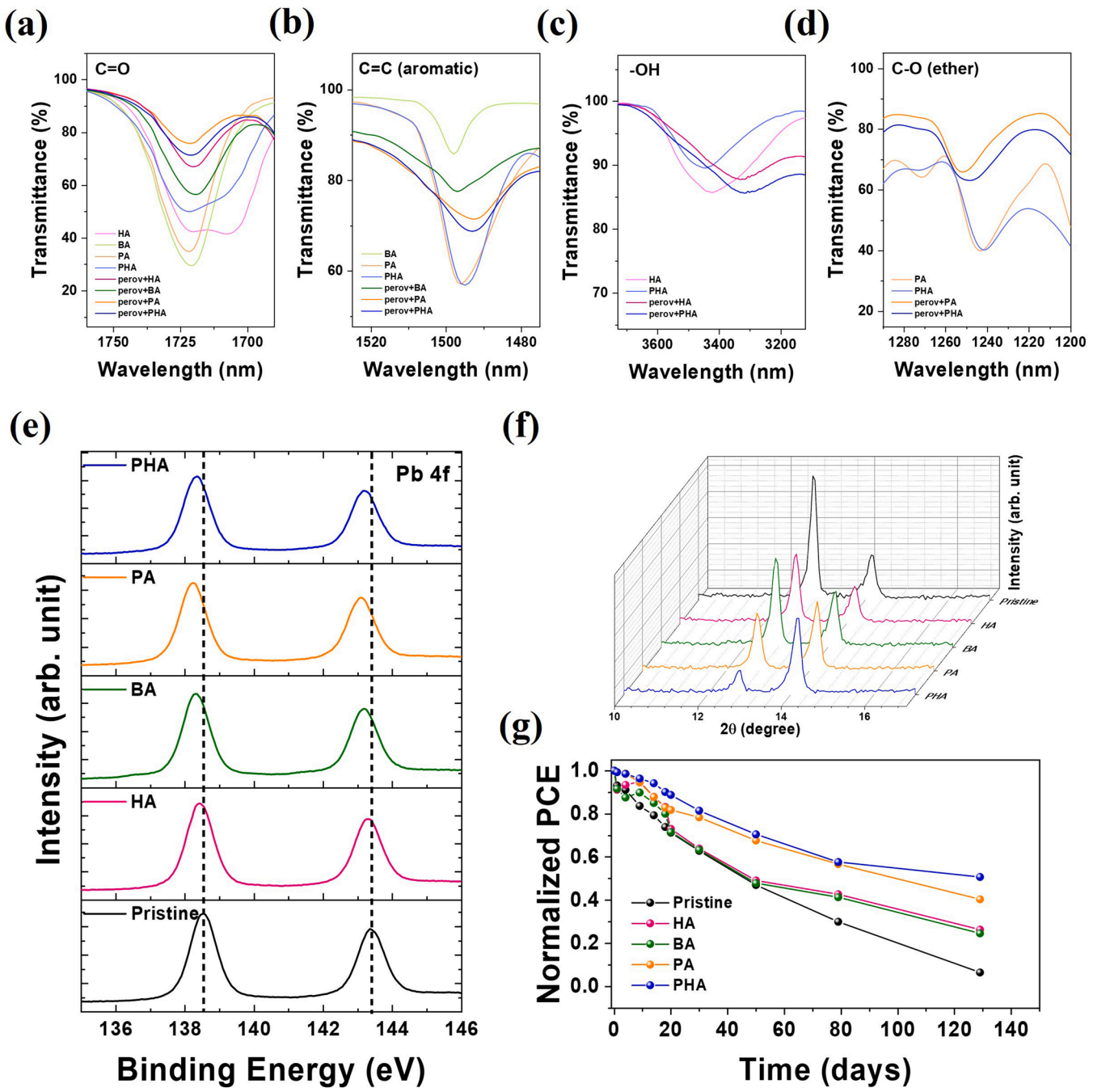

Fig. 5. FT-IR spectra of HA, BA, PA, and PHA with and without perovskite precursor in expanded fingerprint region for (a) 1760–1690 cm^{-1}, (b) 1525–1475 cm^{-1}, (c) 3730–3120 cm^{-1}, and (d) 1290–1200 cm^{-1}. XPS spectra of (e) Pb 4 f peaks of perovskite films with and without different passivation molecules. (f) XRD patterns of perovskite films with and without different passivation molecules after 70 days under ambient air condition with RH 45 ± 5%. (g) Stability test results for normalized PCE of devices with and without different passivation molecules under ambient air condition (25 ± 5 ℃, 45 ± 5%~55 ± 5% RH).

of humidity aging, the pristine shows a prominent PbI_2 peak (001) at about 12.7° caused by the deterioration of perovskite, while the perovskite films that have adopted passivation molecules show a markedly lower intensity of the PbI_2 peak (001) along with a higher perovskite (110) peak intensity. The lower (001)/(110) values for Pristine, HA, BA, PA, and PHA (2.50, 1.68, 1.54, 0.83, and 0.38, respectively) indicate improved humidity stability, which results from the increased moisture resistance due to the introduction of functional groups and better morphology. We secondly tested the sensitivity to oxygen and moisture of PSCs with and without multifunctional molecules without encapsulation under 50 ± 10% RH at 30 ± 5 ℃ (Figs. 5g, S7). As shown in Fig. 5g, the devices with HA, BA, PA, and PHA respectively maintained 19%, 18%, 34%, and 38% of their initial PCE values after 189 days; meanwhile the control devices only retained 0% of their initial efficiency after the same period of time and under the same conditions. The slower PCE-reduction shown in PSCs with multifunctional molecules could be due to the enhanced perovskite film-quality as a result of not only the reduced defects induced by the multifunctional molecules being able to passivate various defects, but also the increased hydrophobic characteristics with a longer alkyl length or benzene ring, which can be confirmed by the increase of water contact angle of the perovskite films with multifunctional additives as shown in Fig. S8 [24,55,56]. Thus, the AAE-adopted multifunctional molecules rendered the PSCs more stable devices with increased

moisture resistance capability along with enhanced cell efficiency. Based on these results, it is reasonable to consider that the perovskite surface is well passivated by well-structured PHA having C═O, –OH, aromatic ring, and C–O functional groups. More specifically, based on the understanding of the passivation mechanism, we guarantee that a new passivation molecule (PHA) containing all four passivation functional groups has the strongest passivation effects; it can therefore be inferred that PHA has much larger passivation effects on the perovskite films when the PHA is introduced by the AAE process, which is also consistent with the prominent increases in PCE, V_{OC}, and stability described above.

The results described above confirm that the multifunction additive engineering strategy effectively eliminates the multi-site defects in polycrystalline perovskite films. This leads to other questions: First, does this PHA work well in other passivation processes? Secondly, which passivation process is the best production method for PSCs? Thirdly, how effectively can the grain boundaries and surface defects be passivated without interfering in the charge carrier mobility? In this work, we experimentally introduced PHA molecules to different locations of the perovskite layer through the following routes: (i) additive engineering (AE: additives are added to the perovskite precursor solution), (ii) antisolvent additive engineering (AAE: additives are introduced into the antisolvent), and (iii) surface post-treatment (SP: additives are introduced into the perovskite surface after perovskite film formation), which are respectively expected to result in GB passivation, surface & GB passivation, and surface-oriented passivation. Figs. 6a and S9 show the photovoltaic characteristic distributions of the PHA-adopted AE, AAE, and SP processes. The PSCs based on PHA all have better performance than conventional perovskite solar cells, and PSCs prepared by both AAE and SP processes showed more increased V_{OC}, probably due to favorable WF changes shown in Fig. S10. [57–59] *Most* importantly, the PHA-based AAE process showed the highest efficiency, which indicates that the PHA introduced by the AAE process is preferable for achieving better perovskite performance. To elucidate the mechanisms behind these results, we conducted a PL measurement to identify the distribution of PHA molecules and passivation effects when incorporated as an additive through various passivation methods. The experimental setup is illustrated in Fig. 6b, and it is recorded under the excitation light from either the film side (FS) or the glass side (GS). The spontaneous radiative recombination via trap states typically resulted in a red-shifted emission compared to that from the band-edge transition, and passivation of these trap states can lead to a blue-shift in the PL peak [15]. As shown in Figs. 6c and S11a–d, at the FS, the perovskite films obtained by AAE and SP displayed strong PL peaks at 792.99 nm and 792.74 nm, respectively, whereas the PL emission of AE showed a relative red-shift to 793.47 nm with a weaker signal. However, at the GS, the PL peaks obtained by AAE and SP displayed relative red-shifts at 794.41 nm and 794.43 nm, respectively, with much weaker signals, while the AE shows similar signals as FS. These phenomena indicated that the AE could uniformly passivate from the bottom to the top of perovskite films, but that it has an insufficient effect, and that when the SP is used, the surface defects are effectively passivated only on the top side. On the other hand, the AAE process intensively eliminates even near-surface defects, while it can also eliminate defects on the bottom side. As a result, the enhanced and blue-shifted PL measurements indicate that the trap states can be successfully minimized using PHA-adopted passivation strategies. Further, the AAE route can significantly passivate the surface defects as well as the bulk of perovskite, with an apparent lower density of trap states and better photovoltaic parameters compared to those obtained using the AE and SP strategy. To elucidate how the PL results above were obtained and examine the substantial depth profile of PHA molecules in perovskite layer according to the different passivation methods, Time-of-Flight Secondary Ion Mass Spectrometer (TOF-SIMS) analysis was conducted, and the element O^- was used as an indicator of PHA (Fig. 6d–g). We measured the distribution of PHA according to depth, and the results showed that O^- gradually decreased over the etching time, ultimately reaching an interval where PbI_2^- began to remain somewhat constant, which is

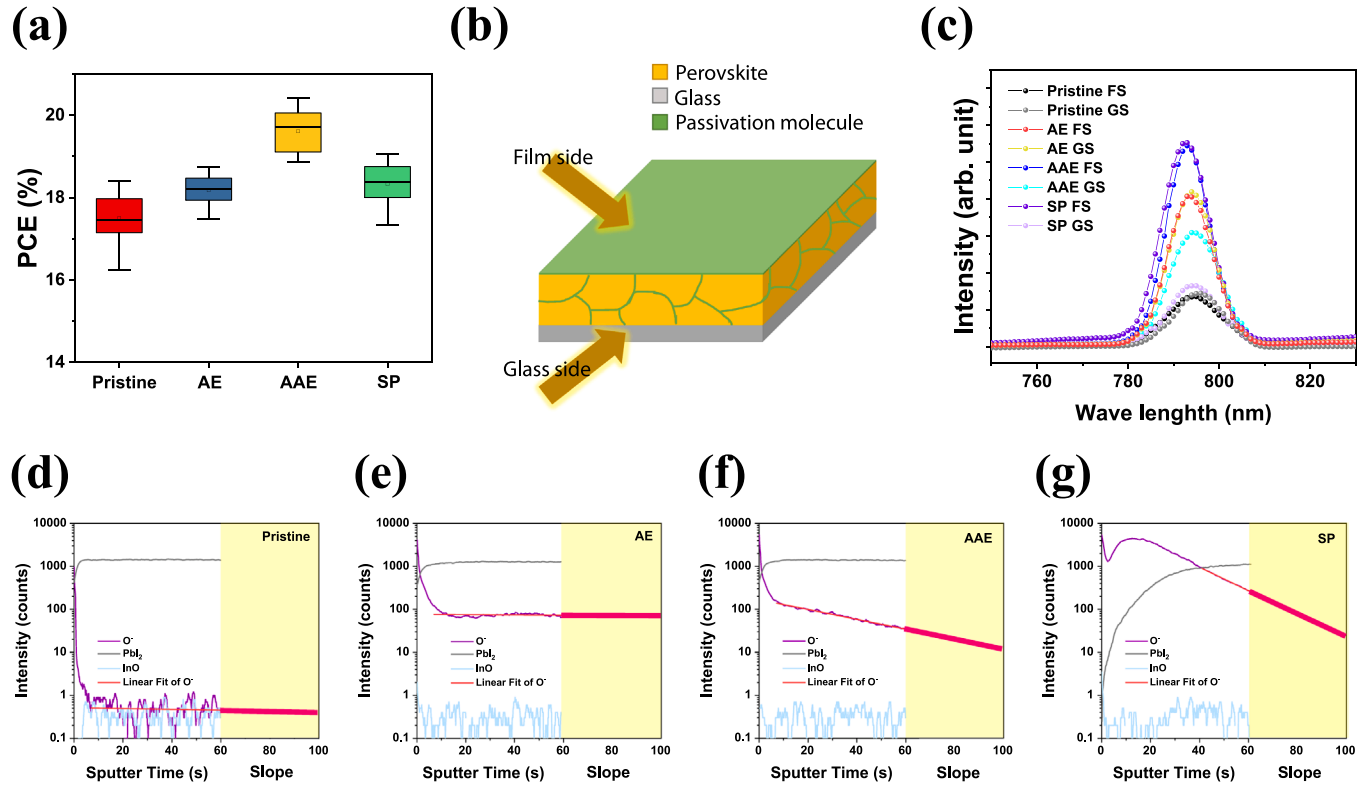

Fig. 6. (a) Statistical distribution of PCE performance for Pristine, AE, AAE, and SP. (b) Schematic image of PL measurement. (c) PL spectra of perovskite films for Pristine, AE, AAE, and SP. TOF-SIMS depth profiles (from surface to bottom) of perovskite films: (d) Pristine, (e) AE, (f) AAE, and (g) SP.

considered to be the influence of the perovskite surface, and the PHA distribution according to the depth inside the bulk was expressed through the slope extrapolation marked with a purple line on the yellow background inset in Fig. 6d–g. In the pristine perovskite film, O^- was not detected in the bulk part, indicating that PHA is not present in the bulk. On the other hand, it was confirmed that PHA exists in the bulk inside the samples prepared using the other passivation processes. The AE process internally has a constant PHA distribution, indicating that PHA are uniformly distributed through the whole depth of the bulk without a concentration gradient. Notably, it was confirmed that PHA gradually decreased from the surface through the AAE process, while the slope of O^- is close to 0 in the AE process, and the slope of O^- in the SP process is much steeper, which represents its abundance on the surface before disappearing rapidly in the bulk in the SP process. Therefore, since the AAE process can penetrate the additive material to some depth inside the perovskite film prior to crystallization and complete the conversion to solid perovskite, it is believed that the PHA-based AAE process could lead to the substantial incorporation of PHA into perovskite with a favorable gradient distribution near the perovskite interface during the crystallization process or before the fully solid-state perovskite film is formed, which was practically and visibly confirmed by the both side PL and SIMS data of Fig. 6. More importantly, based on these new findings and consideration (1), AAE has more a favorable and appropriate gradient distribution of additives, and AAE can more effectively passivate the defects in both bulk and surface than the two conventional processes (AE, SP). (2) The additive's gradient distribution can be more effective for the charge transport capability than the more surface or bulk-oriented additive's distribution due to the generally known insulating nature of used additives [19,20]; it can therefore be concluded that this novel and favorable PHA-adopted AAE process can be considered to provide a more effective and convenient way to obtain high quality perovskite films, thus ensuring the creation of high-performance PSCs with higher PCE and more long-term stability.

3. Conclusion

In summary, we have introduced new multi-functional additives (HA, BA, PA, and PHA) including C═O, –OH, –O–CH_2, or aromatic functional groups to obtain highly efficient and stable PSCs. We then comprehensively investigated the operation and strength of each functional group as well as its role and effects on the photovoltaic performance of perovskite films. We determined that the effective multi-functional passivation molecules significantly improved the perovskite grain size and crystal growth as well as the charge carrier extraction and transport, thus resulting in remarkably improved device performance. Further, depending on the positions and types of functional groups in the molecule, we investigated whether it works in the perovskite and the chemical bond. Using PHA, it was revealed that the four functional groups of PHA can strongly interact with positively and negatively charged defects such as undercoordinated Pb^{2+}, organic cations, and halogen anions; it was also revealed that the hydrophobic long alkyl chain and benzene ring effectively prevent degradation for perovskite films more than other passivation molecules because they have the most synergetic effects of functional groups, which could also be responsible for the improved efficiency and stability. More interestingly, we found that the facile and novel AAE treatment passivates not only the surface but also some bulk defects, and we further revealed that the proper gradient-slope of the actual additive distribution within the perovskite layer via AAE can improve the passivation effect and the charge transfer more effectively than the conventional passivation methods. As a result, the optimal device made using PHA-adopted AAE showed a significant increase in V_{OC} from 1.069 V to 1.153 V, achieving the highest efficiency of 20.72%. The stability of PSCs using PHA was also improved. Our finding provides an enhanced passivation molecule structure and a practical approach for producing high quality perovskite films with high PCE and long-term stability.

4. Experimental

4.1. Materials

Indium tin oxide (ITO) glass (10 Ω sq^{-1}, 1.5 ×1.5 cm) was purchased from AMG-Tech. Nickel oxide nanoparticles in ethanol (NiO NPs, 2.5 wt %), Zinc oxide nanoparticles in 2-propanol (ZnO NPs, 2.5 wt%), and phenyl-C_{61}-butyric acid methyl ester ($PC_{61}BM$) were all purchased from 1-Material. Formamidinium iodide (FAI, 98%) was purchased from Great Cell Solar. Lead iodide (PbI_2, 99%), lead bromide ($PbBr_2$, 99%), and benzyl acrylate (BA) were all purchased from Tokyo Chemical Industry. Methylammonium bromide (MABr, ≥99), cesium iodide (CsI, 99.99%), N,N-dimethylformamide (DMF, 99.8%), dimethyl sulfoxide (DMSO, 99.7%), chlorobenzene (CB), toluene (TL, 99.8%), iso propyl alcohol (IPA), 2-hydroxyethyl acrylate (HA), 2-Phenoxyethyl acrylate (PA), and 3-Phenoxy-2-hydroxypropyl acrylate (PHA) were all purchased from Sigma-Aldrich.

4.2. Device fabrication

First, the pre-dopped ITO substrates were cleaned by ultrasonication with deionized water, acetone, and IPA for 10 min, respectively. After drying, the substrates were treated with UV-ozone for 20 min. To prepare the hole-transporting layer (HTL), NiO NPs (40 μL) solution was spin-coated onto the UV-treated ITO substrate at 4000 rpm for 40 s, after which the films were heated at 350 ℃ for 30 min. For the tri-cation perovskite ($Cs_{0.175}FA_{0.750}MA_{0.075}Pb(I_{0.880}Br_{0.120})_3$, 48 wt%) layer, the perovskite precursor solution was prepared by dissolving 568 mg PbI_2, 80 mg $PbBr_2$, 187 mg FAI, 66 mg CsI, and 12 mg MABr in 1.0 ml of mixed solvent in a 4:1 vol ratio (DMF:DMSO), respectively. Then, the perovskite solution (35 μL) was spin-coated by a 2-step process onto the ITO/NiO NPs substrate at 500 rpm for 5 s and at 5000 rpm for 45 s. Thirty seconds before the end of the 2-step spin coating, TL (0.4 ml) was dripped onto the substrate, and the substrate was then heated at 100 ℃ for 30 min. To prepare the AAE process, we added HA, BA, PA, and PHA to TL with the optimal concentration of each molecule (1 vol%, 0.1 vol %, 0.1 vol%, and 0.1 vol%, respectively). To compare the three passivation methods—additive engineering (AE), antisolvent additive engineering (AAE), and surface post-treatment (SP)—PHA was added in perovskite precursor, toluene-based anti-solvent, and IPA with the 0.1 vol%. Instead of pristine perovskite solution, the AE method was applied with PHA-added perovskite solution (35 μL) dripped onto the ITO/NiO NPs substrate, then coated and heat-treated in the same way. Next, after the perovskite annealing, the SP method for surface passivation was performed. PHA-added IPA solution (30 μL) was spin-coated onto the ITO/NiO NPs/Perovskite substrate at 4000 rpm for 30 s, after which the films were heated at 100 ℃ for 10 min. To prepare the electron-transporting layer (ETL), $PC_{61}BM$ solution was prepared by dissolving 20 mg $PC_{61}BM$ in 1.0 ml of CB, and this solution (20 μL) was then spin-coated onto the ITO/NiO NPs/Perovskite substrate at 6000 rpm for 50 s, after which the films were heated at 100 ℃ for 10 min. Next, the ZnO NPs (30 μL) was spin-coated using a 2-step process onto the ITO/NiO NPs/Perovskite/PCBM substrate at 1000 rpm for 15 s and at 8000 rpm for 40 s, after which the substrates were annealed at 100 ℃ for 10 min. Finally, the top electrode (Ag 100 nm, active area 0.0464 cm^2) was deposited on the top of the sample in a thermal evaporation chamber under vacuum conditions (10^{-6} torr).

4.3. Device and film characterization

The photocurrent density-voltage (J-V) characteristics were taken using appropriate measurement units (Keithley 2400 and Oriel solar (Class AAA) simulator) under Air Mass 1.5 G, and the light intensity was calibrated using a standard Si reference cell certified by the International System of Units (SI) (SRC 1000 TC KG5N, VLSI Standards, Inc). The dependency of V_{OC} on light intensity was determined by controlling

the neutral density (ND) filter wheel (Newport). The external quantum efficiency (EQE) and internal quantum efficiency (IQE) were recorded using a quantum efficiency measurement system (IQE-200, Oriel Instruments, USA) under monochromatic illumination. The photo-generated charge carrier extraction by linearly increasing voltage (photo-CELIV), transient photo-voltage (TPV), and transient photo-current (TPC) measurements were conducted using a multi-functional organic semiconductor parameter test system (T4000, McScience) including a Tektronix oscilloscope (DPO-2014B) with a 100 MHz bandwidth. The X-ray diffraction (XRD) was obtained by a RIGAKU D/MAX 2500 powder diffractometer with $2\theta = 10–40^{\circ}$ under Cu Ka radiation. The surface and cross-section images of the perovskite films were analyzed using a field-emission scanning electron microscope (FE-SEM, SU8220, HITACHI). Ultraviolet-visible spectroscopy (UV–vis) measurements were obtained using a UV–vis spectrophotometer (HP, Hewlett Packard). Steady-state photoluminescence (PL, RF-6000, SHIMADZU) was obtained under excitation wavelength of 398 nm and scan speed 2000 nm/min. Atomic force microscopy (AFM) was measured as well (XE7, Park System). Fourier-transform infrared spectrometry (FT-IR) was performed in the range from 4000–1000 cm^{-1} (Frontier, PerkinElmer model). The chemical compositions and interactions of the perovskite films were confirmed using an X-ray photoelectron spectrometer (XPS, K-Alpha+, Thermo Fisher Scientific), and a Time-of-Flight Secondary Ion Mass Spectrometer (TOF-SIMS, M6, IONTOF GmbH) was used to analyze the composition according to the depth in the perovskite layer.

Declaration of Competing Interest

The authors declare that they have no known competing financial interests or personal relationships that could have appeared to influence the work reported in this paper.

Acknowledgements

This research was supported by the Basic Science Research Program through the National Research Foundation of Korea (NRF), funded by the Ministry of Education (2021R1A2C2010353).

Appendix A. Supporting information

Supplementary data associated with this article can be found in the online version at doi:10.1016/j.nanoen.2022.107193.

References

[1] A. Kojima, K. Teshima, Y. Shirai, T. Miyasaka, Organometal halide perovskites as visible-light sensitizers for photovoltaic cells, J. Am. Chem. Soc. 131 (2009) 6050–6051.
[2] P. Umari, E. Mosconi, F. De Angelis, Infrared dielectric screening determines the low exciton binding energy of metal-halide perovskites, J. Phys. Chem. Lett. 9 (2018) 620–627.
[3] X. Li, F. Cao, D. Yu, J. Chen, Z. Sun, Y. Shen, Y. Zhu, L. Wang, Y. Wei, Y. Wu, All inorganic halide perovskites nanosystem: synthesis, structural features, optical properties and optoelectronic applications, Small 13 (2017), 1603996.
[4] NREL, Best Research-Cell Efficiencies, National Renewable Energy Laboratory, 2021, ⟨https://www.nrel.gov/pv/assets/pdfs/best-research-cell-efficiencies-rev211214.pdf⟩.
[5] N.J. Jeon, J.H. Noh, W.S. Yang, Y.C. Kim, S. Ryu, J. Seo, S.I. Seok, Compositional engineering of perovskite materials for high-performance solar cells, Nature 517 (2015) 476–480.
[6] G. Hodes, Perovskite-based solar cells, Science 342 (2013) 317–318.
[7] G. Xing, N. Mathews, S. Sun, S.S. Lim, Y.M. Lam, M. Grätzel, S. Mhaisalkar, T. C. Sum, Long-range balanced electron-and hole-transport lengths in organic-inorganic CH3NH3PbI3, Science 342 (2013) 344–347.
[8] Y. Zhao, K. Zhu, Organic–inorganic hybrid lead halide perovskites for optoelectronic and electronic applications, Chem. Soc. Rev. 45 (2016) 655–689.
[9] B. Chen, P.N. Rudd, S. Yang, Y. Yuan, J. Huang, Imperfections and their passivation in halide perovskite solar cells, Chem. Soc. Rev. 48 (2019) 3842–3867.
[10] Z. Liu, L.K. Ono, Y. Qi, Additives in metal halide perovskite films and their applications in solar cells, J. Energy Chem. 46 (2020) 215–228.
[11] L. Fu, H. Li, L. Wang, R. Yin, B. Li, L. Yin, Defect passivation strategies in perovskites for an enhanced photovoltaic performance, Energy Environ. Sci. 13 (2020) 4017–4056.
[12] S. Liu, Y. Guan, Y. Sheng, Y. Hu, Y. Rong, A. Mei, H. Han, A review on additives for halide perovskite solar cells, Adv. Energy Mater. 10 (2020), 1902492.
[13] F. Zhang, K. Zhu, Additive engineering for efficient and stable perovskite solar cells, Adv. Energy Mater. 10 (2020), 1902579.
[14] T. Li, Y. Pan, Z. Wang, Y. Xia, Y. Chen, W. Huang, Additive engineering for highly efficient organic–inorganic halide perovskite solar cells: recent advances and perspectives, J. Mater. Chem. A 5 (2017) 12602–12652.
[15] S. Yang, J. Dai, Z. Yu, Y. Shao, Y. Zhou, X. Xiao, X.C. Zeng, J. Huang, Tailoring passivation molecular structures for extremely smallopen-circuit voltage loss in perovskite solar cells, J. Am. Chem. Soc. 141 (2019) 5781–5787.
[16] G. Liu, H. Zheng, L. Zhang, H. Xu, S. Xu, X. Xu, Z. Liang, X. Pan, Tailoring multifunctional passivation molecules with halogen functional groups for efficient and stable perovskite photovoltaics, Chem. Eng. J. 407 (2021), 127204.
[17] L. Zhang, K. Cao, J. Qian, Y. Huang, X. Wang, M. Ge, W. Shen, F. Huang, M. Wang, W. Zhang, Crystallization control and multisite passivation of perovskites with amino acid to boost the efficiency and stability of perovskite solar cells, J. Mater. Chem. C 8 (2020) 17482–17490.
[18] Y. Wu, X. Yang, W. Chen, Y. Yue, M. Cai, F. Xie, E. Bi, A. Islam, L. Han, Perovskite solar cells with 18.21% efficiency and area over 1 cm2 fabricated by heterojunction engineering, Nat. Energy 1 (2016) 1–7.
[19] Y.-H. Wu, X.-Q. Shi, X.-H. Ding, Y.-K. Ren, T. Hayat, A. Alsaedi, Y. Ding, P. Xu, S.-Y. Dai, Incorporating 4-tert-butylpyridine in an antisolvent: a facile approach to obtain highly efficient and stable perovskite solar cells, ACS Appl. Mater. Interfaces 10 (2018) 3602–3608.
[20] X. Li, C.C. Chen, M. Cai, X. Hua, F. Xie, X. Liu, J. Hua, Y.T. Long, H. Tian, L. Han, Efficient passivation of hybrid perovskite solar cells using organic dyes with COOH functional group, Adv. Energy Mater. 8 (2018), 1800715.
[21] Y. Huang, T. Liu, B. Wang, J. Li, D. Li, G. Wang, Q. Lian, A. Amini, S. Chen, C. Cheng, Antisolvent engineering to optimize grain crystallinity and hole-blocking capability of perovskite films for high-performance photovoltaics, Adv. Mater. 33 (2021), 2102816.
[22] X. Li, S. Ke, X. Feng, X. Zhao, W. Zhang, J. Fang, Enhancing the stability of perovskite solar cells through cross-linkable and hydrogen bonding multifunctional additives, J. Mater. Chem. A 9 (2021) 12684–12689.
[23] Y. Li, J. Shi, J. Zheng, J. Bing, J. Yuan, Y. Cho, S. Tang, M. Zhang, Y. Yao, C.F. J. Lau, Acetic acid assisted crystallization strategy for high efficiency and long-term stable perovskite solar cell, Adv. Sci. 7 (2020), 1903368.
[24] L. Zhu, X. Zhang, M. Li, X. Shang, K. Lei, B. Zhang, C. Chen, S. Zheng, H. Song, J. Chen, Trap state passivation by rational ligand molecule engineering toward efficient and stable perovskite solar cells exceeding 23% efficiency, Adv. Energy Mater. 11 (2021), 2100529.
[25] J. Zhuang, P. Mao, Y. Luan, X. Yi, Z. Tu, Y. Zhang, Y. Yi, Y. Wei, N. Chen, T. Lin, Interfacial passivation for perovskite solar cells: the effects of the functional group in phenethylammonium iodide, ACS Energy Lett. 4 (2019) 2913–2921.
[26] S. Ning, S. Zhang, J. Sun, C. Li, J. Zheng, Y.M. Khalifa, S. Zhou, J. Cao, Y. Wu, Ambient pressure x-ray photoelectron spectroscopy investigation of thermally stable halide perovskite solar cells via post-treatment, ACS Appl. Mater. Interfaces 12 (2020) 43705–43713.
[27] Y.-H. Seo, J.-S. Yeo, N. Myoung, S.-Y. Yim, M. Kang, D.-Y. Kim, S.-I. Na, Blending of n-type semiconducting polymer and PC61BM for an efficient electron-selective material to boost the performance of the planar perovskite solar cell, ACS Appl. Mater. Interfaces 8 (2016) 12822–12829.
[28] M.-J. Choi, Y.-S. Lee, I.H. Cho, S.S. Kim, D.-H. Kim, S.-N. Kwon, S.-I. Na, Functional additives for high-performance inverted planar perovskite solar cells with exceeding 20% efficiency: selective complexation of organic cations in precursors, Nano Energy 71 (2020), 104639.
[29] J. Zhen, W. Zhou, M. Chen, B. Li, L. Jia, M. Wang, S. Yang, Pyridine-functionalized fullerene additive enabling coordination interactions with CH3NH3PbI3 perovskite towards highly efficient bulk heterojunction solar cells, J. Mater. Chem. A 7 (2019) 2754–2763.
[30] Y. Yang, H. Peng, C. Liu, Z. Arain, Y. Ding, S. Ma, X. Liu, T. Hayat, A. Alsaedi, S. Dai, Bi-functional additive engineering for high-performance perovskite solar cells with reduced trap density, J. Mater. Chem. A 7 (2019) 6450–6458.
[31] Y. Huang, S. Wu, R. Chen, S. Fang, S. Zhang, G. Wang, W. Chen, Efficient methylamine-containing antisolvent strategy to fabricate high-efficiency and stable FA0.85Cs0.15Pb(Br0.15I2.85) perovskite solar cells, ACS Appl. Mater. Interfaces 11 (2019) 18415–18422.
[32] J. Peng, Y. Chen, K. Zheng, T. Pullerits, Z. Liang, Insights into charge carrier dynamics in organo-metal halide perovskites: from neat films to solar cells, Chem. Soc. Rev. 46 (2017) 5714–5729.
[33] Y. Chen, J. Peng, D. Su, X. Chen, Z. Liang, Efficient and balanced charge transport revealed in planar perovskite solar cells, ACS Appl. Mater. Interfaces 7 (2015) 4471–4475.
[34] Y. Guo, H. Lei, L. Xiong, B. Li, G. Fang, An integrated organic–inorganic hole transport layer for efficient and stable perovskite solar cells, J. Mater. Chem. A 6 (2018) 2157–2165.
[35] A.E. Shalan, E. Akman, F. Sadegh, S. Akin, Efficient and stable perovskite solar cells enabled by dicarboxylic acid-supported perovskite crystallization, J. Phys. Chem. Lett. 12 (2021) 997–1004.
[36] X. Hou, S. Huang, W. Ou-Yang, L. Pan, Z. Sun, X. Chen, Constructing efficient and stable perovskite solar cells via interconnecting perovskite grains, ACS Appl. Mater. Interfaces 9 (2017) 35200–35208.

[37] S. Yuan, F. Qian, S. Yang, Y. Cai, Q. Wang, J. Sun, Z. Liu, S. Liu, NbF5: a novel α-phase stabilizer for FA-based perovskite solar cells with high efficiency, Adv. Funct. Mater. 29 (2019), 1807850.
[38] S. Wang, Z. Ma, B. Liu, W. Wu, Y. Zhu, R. Ma, C. Wang, High-performance perovskite solar cells with large grain-size obtained by using the Lewis acid-base adduct of thiourea, Sol. RRL 2 (2018), 1800034.
[39] N. Li, F. Xu, Z. Qiu, J. Liu, X. Wan, X. Zhu, H. Yu, C. Li, Y. Liu, B. Cao, Sealing the domain boundaries and defects passivation by Poly (acrylic acid) for scalable blading of efficient perovskite solar cells, J. Power Sources 426 (2019) 188–196.
[40] Y. Guo, J. Ma, H. Lei, F. Yao, B. Li, L. Xiong, G. Fang, Enhanced performance of perovskite solar cells via anti-solvent nonfullerene Lewis base IT-4F induced trap-passivation, J. Mater. Chem. A 6 (2018) 5919–5925.
[41] Y. Shao, Z. Xiao, C. Bi, Y. Yuan, J. Huang, Origin and elimination of photocurrent hysteresis by fullerene passivation in CH3NH3PbI3 planar heterojunction solar cells, Nat. Commun. 5 (2014) 1–7.
[42] Y.-J. Kang, S.-N. Kwon, S.-P. Cho, Y.-H. Seo, M.-J. Choi, S.-S. Kim, S.-I. Na, Antisolvent additive engineering containing dual-function additive for triple-cation p–i–n perovskite solar cells with over 20% PCE, ACS Energy Lett. 5 (2020) 2535–2545.
[43] C. Ma, N.-G. Park, Paradoxical approach with a hydrophilic passivation layer for moisture-stable, 23% efficient perovskite solar cells, ACS Energy Lett. 5 (2020) 3268–3275.
[44] J. Li, X. Hua, F. Gao, X. Ren, C. Zhang, Y. Han, Y. Li, B. Shi, S.F. Liu, Green antisolvent additive engineering to improve the performance of perovskite solar cells, J. Energy Chem. 66 (2022) 1–8.
[45] J. Peng, J.I. Khan, W. Liu, E. Ugur, T. Duong, Y. Wu, H. Shen, K. Wang, H. Dang, E. Aydin, A universal double-side passivation for high open-circuit voltage in perovskite solar cells: role of carbonyl groups in poly (methyl methacrylate), Adv. Energy Mater. 8 (2018), 1801208.
[46] H. Zheng, L. Zhu, L. Hu, S. Yang, S. Chen, A. Alsaedi, T. Hayat, Y. Huang, X. Pan, S. Dai, Promoting perovskite crystal growth to achieve highly efficient and stable solar cells by introducing acetamide as an additive, J. Mater. Chem. A 6 (2018) 9930–9937.
[47] S.-P. Cho, S.-N. Kwon, M.-J. Choi, Y.-H. Seo, S.-S. Kim, S.-I. Na, Enhanced device performances of MAFACsPb(IxBr1–x) perovskite solar cells with dual-functional 2-chloroethyl acrylate additives, ACS Appl. Mater. Interfaces 12 (2020) 46846–46853.
[48] J. Chen, S.-G. Kim, X. Ren, H.S. Jung, N.-G. Park, Effect of bidentate and tridentate additives on the photovoltaic performance and stability of perovskite solar cells, J. Mater. Chem. A 7 (2019) 4977–4987.
[49] S.-H. Lee, S. Jeong, S. Seo, H. Shin, C. Ma, N.-G. Park, Acid dissociation constant: a criterion for selecting passivation agents in perovskite solar cells, ACS Energy Lett. 6 (2021) 1612–1621.
[50] D.-H. Kang, S.-Y. Kim, J.-W. Lee, N.-G. Park, Efficient surface passivation of perovskite films by a post-treatment method with a minimal dose, J. Mater. Chem. A 9 (2021) 3441–3450.
[51] H. Jiang, Z. Yan, H. Zhao, S. Yuan, Z. Yang, J. Li, B. Liu, T. Niu, J. Feng, Q. Wang, Bifunctional hydroxylamine hydrochloride incorporated perovskite films for efficient and stable planar perovskite solar cells, ACS Appl. Energy Mater. 1 (2018) 900–909.
[52] K. Zhu, S. Cong, Z. Lu, Y. Lou, L. He, J. Li, J. Ding, N. Yuang, M.H. Rümmeli, G. Zou, Enhanced perovskite solar cell performance via defect passivation with ethylamine alcohol chlorides additive, J. Power Sources 428 (2019) 82–87.
[53] Z. Zhang, Y. Gao, Z. Li, L. Qiao, Q. Xiong, L. Deng, Z. Zhang, R. Long, Q. Zhou, Y. Du, Z. Lan, Y. Zhao, C. Li, K. Mullen, P. Gao, Marked passivation effect of naphthalene-1,8-dicarboximides in high-performance perovskite solar cells, Adv. Mater. 33 (2021), e2008405.
[54] D. Wei, F. Ma, R. Wang, S. Dou, P. Cui, H. Huang, J. Ji, E. Jia, X. Jia, S. Sajid, Ion-migration inhibition by the cation–π interaction in perovskite materials for efficient and stable perovskite solar cells, Adv. Mater. 30 (2018), 1707583.
[55] H. Li, J. Shi, J. Deng, Z. Chen, Y. Li, W. Zhao, J. Wu, H. Wu, Y. Luo, D. Li, Intermolecular π–π conjugation self-assembly to stabilize surface passivation of highly efficient perovskite solar cells, Adv. Mater. 32 (2020), 1907396.
[56] W. Zhao, J. Xu, K. He, Y. Cai, Y. Han, S. Yang, S. Zhan, D. Wang, Z. Liu, S. Liu, A special additive enables all cations and anions passivation for stable perovskite solar cells with efficiency over 23, Nanomicro Lett. 13 (2021) 169.
[57] P. Patil, D.S. Mann, S.R. Rondiya, N.Y. Dzade, S.-N. Kwon, S.-I. Na, Enhanced performance of perovskite solar cells via reactive post-treatment process utilizing guanidine acetate as interface modifier, Sol. RRL 5 (2021), 2100547.
[58] Y. Cai, J. Cui, M. Chen, M. Zhang, Y. Han, F. Qian, H. Zhao, S. Yang, Z. Yang, H. Bian, Multifunctional enhancement for highly stable and efficient perovskite solar cells, Adv. Funct. Mater. 31 (2021), 2005776.
[59] Y. Han, H. Zhao, C. Duan, S. Yang, Z. Yang, Z. Liu, S. Liu, Controlled n-doping in air-stable CsPbI2Br perovskite solar cells with a record efficiency of 16.79%, Adv. Funct. Mater. 30 (2020), 1909972.

Yu-Jin Kang received her M.S. degree in Flexible and Printable Electronics from Jeonbuk National University, Korea in 2021. Currently, she is a researcher at KEPCO (Korea Electric Power Corporation) Research Institute, focusing on high-performance perovskite solar cells and their application including large-area, semi-transparent, and building integrated photovoltaics.

Seok-In Na received his Ph.D. degree in Materials Science and Engineering from the Gwangju Institute of Science and Technology (GIST), South Korea, in 2010. From 2009–2012, he worked as a researcher and a senior researcher at the Korea Institute of Science and Technology (KIST). Since 2012, he has been a professor in the Professional Graduate School of Flexible and Printable Electronics at Jeonbuk National University. His research interests include advanced photoelectronics, novel materials and devices for high-performance solar cells, and flexible and printable electronic devices.